



Combining Carbon Nanoparticle Coatings and Laser Surface Texturing for Enhanced Lubricity Under High Loads

T. MacLucas¹ · P. G. Grützmacher² · P. Leonhard-Trautmann¹ · S. Suarez¹ · C. Gachot² · F. Mücklich¹

Received: 5 September 2023 / Accepted: 30 January 2024 / Published online: 11 March 2024
© The Author(s) 2024

Abstract

Developing new lubrication concepts greatly contributes to improving the energy efficiency of mechanical systems. Nanoparticles such as those based on carbon allotropes or 2D materials have received widespread attention due to their outstanding mechanical and tribological performance. However, these systems are limited by a short wear life. Combining nanoparticle coatings with laser surface texturing has been demonstrated to substantially improve their durability due to the reservoir effect which prevents immediate particle removal from the contact. In this study, we investigate the high-load (20 N) tribological performance of AISI 304 austenitic stainless-steel substrates, which are line-patterned by laser interference patterning and subsequently coated with different carbon nanoparticle coatings (carbon nanotubes, carbon onions, carbon nanohorns) against alumina and 100Cr6 counter bodies. In addition to that, benchmark testing is performed with conventional solid lubricant coatings (graphite, MoS₂, WS₂). Electrophoretic deposition is used as the main coating technique along with air spraying (for WS₂). All coatings substantially improve friction compared to the purely laser-patterned reference. Among all coating materials, carbon nanotubes demonstrate superior lubricity and the longest wear life against 100Cr6 and alumina counter bodies. Detailed characterization of the resulting wear tracks by energy-dispersive X-ray spectroscopy, scanning electron microscopy, and confocal laser scanning microscopy provides insights into the friction mechanisms of the various solid lubricant particles. Further, material transfer is identified as an important aspect for effective and long-lasting lubrication.

Keywords Solid lubricant coatings · Carbon nanotubes · Carbon onions · Carbon nanohorns · Conventional solid lubricants · High load tribometry

1 Introduction

The development of advanced lubrication systems has been an important aspect of modern engineering, as it plays a crucial role in improving the efficiency and durability of mechanical systems, which directly affects overall energy consumption and CO₂ emissions [1]. For many applications, the typically used liquid lubricants are not suitable due to their limited temperature stability or problems related to

their evaporation or to contamination [2, 3]. Therefore, solid lubricants in particular have attracted significant attention due to their excellent lubrication properties, high thermal stability and resistance to oxidation, evaporation, and corrosion. Typical solid lubricants are based on polymers (e.g., PTFE [4]), soft metals (e.g., gold [5]) or 2D materials (e.g., graphite [6], transition metal dichalcogenides (TMD) [7, 8] and MXenes [9]).

In recent years, carbon nanoparticles have emerged as promising candidates for solid lubrication, particularly in the form of coatings [10–12]. Carbon nanoparticles combine unique physical and chemical properties, such as high strength, low density, and high conductivity [13]. The mechanical stability stemming from the combination of mechanical strength with cylindrical (CNT), respectively, spherical (CO, CNH) shapes and a layered morphology (CNT and CO) makes these particles highly interesting for bearing high loads.

✉ T. MacLucas
timothy.maclucas@uni-saarland.de

✉ C. Gachot
Carsten.gachot@tuwien.at

¹ Chair of Functional Materials, Saarland University, Campus D3.3, 66123 Saarbrücken, Germany

² Institute for Engineering Design and Product Development, Research Unit Tribology, TU Wien, Lehnárgasse 6, 1060 Vienna, Austria

However, a major issue for many solid lubricant coatings is a lack of substrate adhesion, which results in a lubricant-depleted contact. This is particularly true for carbon nanoparticles as they don't form covalent bonds with metallic substrates during the coating process [12]. This shortcoming can be tackled by the introduction of surface textures, as those fabricated by laser surface texturing. Laser surface texturing has also gained considerable attention as a technique for improving the tribological properties of metallic surfaces and solid lubricant coatings [2, 3, 12]. During sliding, micro and nano-scale surface features on the substrate material act as lubricant reservoirs and trap wear particles, thus reducing friction and wear [14–16]. A particularly effective technique to create laser textures in the lower μm -scale is direct laser interference patterning (DLIP), which is based on the interference of two or more high-power laser beams [17]. Upon overlapping the laser beams on the surface of the target, material is directly ablated at the so-called interference maxima positions, resulting in the generation of periodic patterns (e.g., lines, cross, or dimples) inside the area of the spot (with diameters of several hundreds of micrometers to several millimeters), even using only a single laser pulse [18]. Additionally, the interaction between laser and material can be tuned by using different laser pulse durations and for ultrashort laser pulses (i.e., pulse duration < 10 ps) the thermal effect on the material is minimal resulting in negligible modification of the material near the created surface textures [19]. When it comes to the combination of laser patterns and solid lubricants, the textures have been shown to store solid lubricant particles in their topographical minima and thus, effectively form reservoirs from where the particles are continuously released into the contact during tribological loading [2, 3, 12, 16]. By creating lubricant-filled reservoirs, the lifetime of the lubrication is significantly extended as the particles are protected from immediate removal from the contact [11, 12, 20].

There are numerous methods to fabricate solid lubricant coatings, such as sputtering [21], burnishing [22], drop casting [23], spray coating [8], and electrophoretic deposition (EPD) [12]. The combination of textured surfaces and coatings applied by EPD is particularly suitable as this process is fast, scalable, offers excellent process control and replicates the laser-induced textures extremely well.

This study investigates the lubricity of carbon nanoparticle coatings (i.e., carbon nanotubes (CNT), carbon onions (CO), and carbon nanohorns (CNH)) on laser patterned AISI304 steel surfaces under high load against 100Cr6 and alumina counter bodies in atmospheric conditions. Additionally, the tribological performance is directly compared to surfaces coated with the widely used solid lubricants graphite, WS_2 , and MoS_2 .

2 Experimental Section

2.1 Materials

As substrate material, mirror-polished austenitic stainless-steel platelets (AISI 304, 20 mm \times 20 mm, 1 mm thick) purchased at Brio Kontrollspiegel GmbH (Germany) was used. Prior to surface patterning and EPD, the platelets were thoroughly rinsed using ultrasonication and cleaned with acetone and isopropanol. Multiwall CNTs were synthesized by chemical vapor deposition (CVD) and purchased at Graphene Supermarket (USA). The particles measure 10–15 μm in length and 30–85 nm diameter. Dahlia-type CNH were purchased from Carbonium SRL (Italy). The clusters measure 60–120 nm in diameter with a single horn diameter of 2–5 nm. COs were fabricated by annealing nanodiamonds (purity $> 98\%$, particle diameter: 4–8 nm, NaBond Technologies Co.) in a vacuum furnace (model 1100-3580-W1, Thermal Technology Inc.) at 1750 $^\circ\text{C}$ for 3 h at a rate of 10 $^\circ\text{C}/\text{min}$ [24]. The graphite powder is a synthetic conducting grade (99.99%, 325 mesh) and was purchased at Alfa Aesar (USA). Both MoS_2 (98%, 325 mesh, which corresponds to 44 μm) and WS_2 (99.8%) powders were purchased from Thermo Scientific (USA).

2.2 Dispersion and Coating Preparation

To prepare for EPD, each dispersion consisted of 70 ml of isopropanol, 10 ml of triethylamine (ACROS Organics, purity: 99%). For the carbon nanoparticles, a concentration of 0.1 mg/ml (solvent) was used, for MoS_2 0.4 mg/ml and for graphite 0.2 mg/ml. Subsequently, the dispersions were subjected to shear mixing (using an Ultra-Turrax IKA T25) and ultrasonication (using a Bandelin Sonorex RK514BH) for 10 min each. During the next step, the substrate and an uncoated AISI 304 platelet (counter electrode) were both immersed in the dispersion and placed parallel to each other. To achieve comparable coating thickness in the 4–5 μm range, the CNTs were deposited for 5 min 45 s, the CNH for 2 min 45 s, the COs for 6 min 15 s, graphite for 4 min 20 s and MoS_2 for 6 min 30 s, all at 300 V. As it is difficult to obtain homogeneous WS_2 coatings via EPD in the 4–5 μm range, air spraying was used as an alternative and 8 ml of WS_2 solution (concentration 28.6 mg/ml) were sprayed onto the substrate.

2.3 Picosecond Direct Laser Interference Patterning

To create line-patterns on the AISI304 substrate platelets (mirror-polished), a Nd:YAG pulsed laser (Edgewave PX-series InnoSlab) integrated into a RDX 500 nano laser

system (Pulsar Photonics GmbH, Germany) was used. The laser operates at a wavelength of 532 nm and the samples were processed at 0.5 W with a pulse duration of 12 ps. The line-patterns were fabricated using two interfering subbeams and have a periodicity (line spacing) of 3.5 μm . To remove superficial contamination such as oxides, the patterned substrates were sonicated in citric acid, acetone and isopropanol for 15 min each.

2.4 Confocal Laser Scanning Microscopy

To assess the depth of the patterns and the coating thicknesses, an Olympus LEXT OLS4100 confocal laser scanning (CLS) microscope was utilized. The microscope is equipped with a 50 \times objective (N.A.: 0.95) and operates at a laser wavelength of 405 nm, providing a vertical resolution of 10 nm and a lateral resolution of 120 nm. R_C (mean height) was used as a measure for the structural depth of the line-patterns over a sampling length of 259 μm . To obtain statistically significant results, R_C was measured for 10 different profile lines on images taken from three distinct spots on the patterned sample surfaces. The coating thickness cannot be measured directly on the patterned surfaces due to their irregularity. For that reason, separate depositions were made on unpatterned surfaces to optimize the deposition parameters so that the coating thickness is 4–5 μm . The optimized parameters were then applied to coat the patterned surfaces, ensuring comparable film thickness.

2.5 Tribometry

Friction testing was conducted on a MFT-2000 tribometer (Rtec, USA) in ball-on-disc setting at a load of 20 N. Measurements were performed in linear reciprocal mode at a stroke length of 1 mm, a velocity of 1 mm/s, and a data acquisition rate of 30 Hz. The sliding direction was perpendicular to the course of the line-pattern. 6 mm balls made from either 100Cr6 steel (Kugel Pompel, Kl.3) or alumina (Kugel Pompel, GD24 which roughly corresponds to an $R_a < 0.045 \mu\text{m}$) were used as counter bodies which corresponds to a Hertzian pressure of 1.78 GPa (100Cr6 vs. AISI 304, with a Young's modulus of 210 GPa for both materials and a Poisson ratio of 0.29 for 100Cr6 and 0.28 for AISI 304) and 2.08 GPa (alumina vs. AISI 304, alumina with a Young's modulus of 375 GPa and a Poisson ratio of 0.25), respectively. Testing was carried out at room temperature and a relative humidity of 25–30%. To ensure statistical representation, each sample was measured three times. The mean COF and the corresponding standard deviations were determined for every single (temporal) measurement point. The raw data was filtered using a Savitzky-Golay filter (25 p) to smooth excessive COF oscillation.

2.6 Wear Track Characterization

To examine the resulting wear tracks, a Helios G4 PFIB CXe dual beam workstation (Thermo Fisher Scientific, USA) with an integrated EDAX detector for energy dispersive x-ray spectroscopy (EDS) was used. Characterization was conducted at a beam current of 1.6 nA and an acceleration voltage of 5 kV. Chemical mapping was performed with 8 cumulative frames.

3 Results and Discussion

3.1 Surface Characterization

The CLS micrographs in Fig. 1 show the top view of the line-patterned AISI 304 steel substrates that were processed by ps-DLIP. Additionally, the images include representative line profiles. To determine R_C , line profiles at various locations were analyzed to obtain a value that is representative of the overall pattern depth. It can be observed that all surfaces have been uniformly patterned, and their line profiles and structural depths are close to identical. These as-processed surfaces were subsequently coated with different solid lubricants.

To ensure comparable coating thickness, the EPD deposition parameters of the CNTs, COs, CNH, graphite, and MoS₂ as well as the solution volume used for air spraying WS₂ were determined such that the resulting thickness of all solid lubricant coatings falls in the 4–5 μm range. Figure 2 shows two sections of each lubricant coating on unpatterned and mirror-polished substrate surfaces. The coating sections are separated by a strip, where the coatings were removed using a soft piece of paper to avoid scratching. Coating thickness is determined by comparing the mean profile height of the left (red rectangle) and right (teal rectangle) coating sections to that of the uncoated strip in the middle (smaller rectangles) as coating thickness cannot be reliably measured directly on line-patterned surfaces. To assess coating uniformity, the profiles belonging to the green lines are shown below the respective micrograph. The identical EPD parameters used for the deposition on unpatterned surfaces were then used to coat the patterned surfaces. As the mean thicknesses of all lubricant coatings is between 4.25 and 5.00 μm , they can be regarded as comparable. Consequently, coating thickness can be neglected as a factor of influence.

3.2 Tribometry and Wear Track Characterization

3.2.1 Counter Body Material: 100Cr6

Figure 3a shows the COF development of the different coatings including an unpatterned and uncoated reference (Ref)

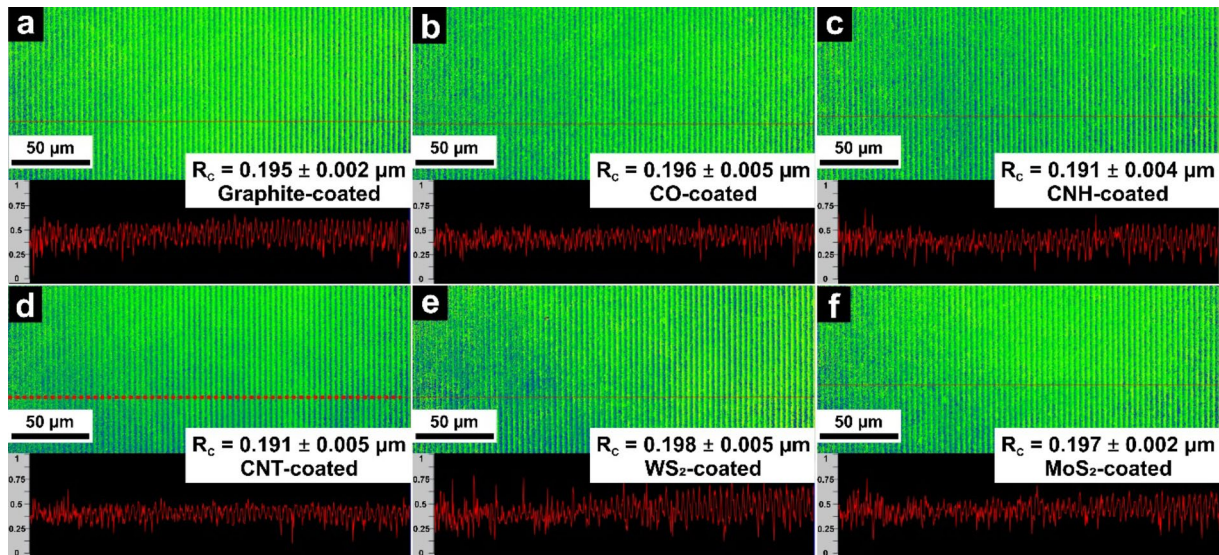


Fig. 1 Top view confocal laser scanning micrographs of the line-patterned AISI 304 substrates which were subsequently coated with **a** graphite, **b** COs, **c** CNH, **d** CNTs, **e** WS_2 , and **f** MoS_2 . In addition

to that, the images show representative line profiles and the overall structural depth (R_c) of the respective pattern

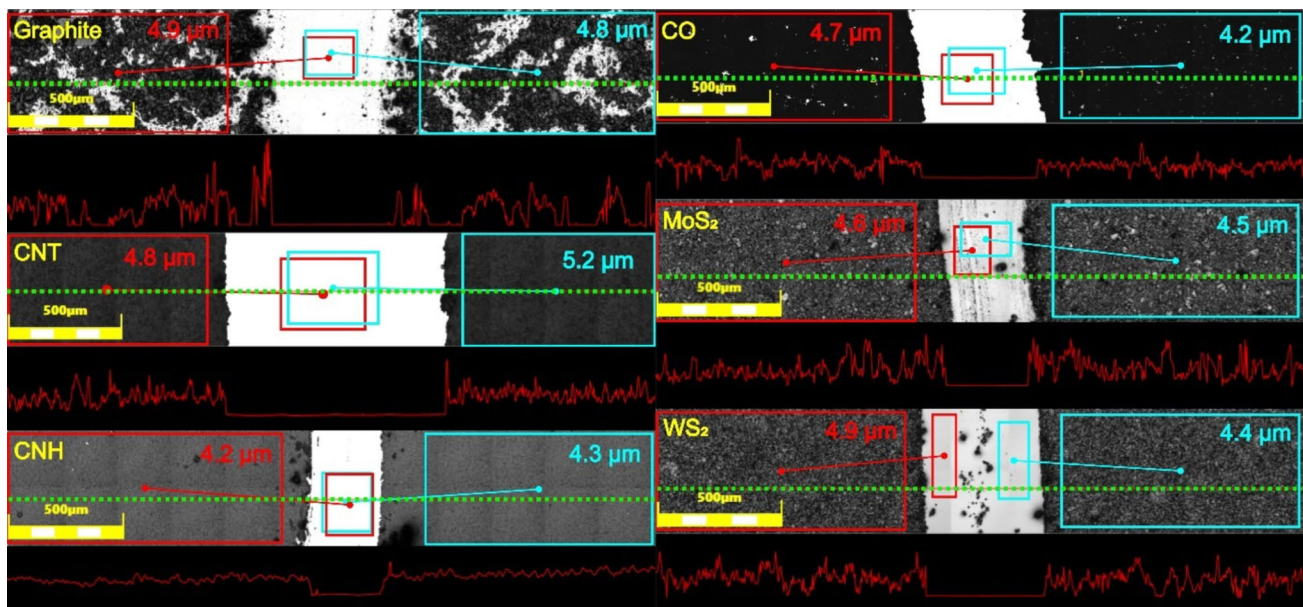


Fig. 2 Top view confocal laser scanning micrographs of the different solid lubricant coatings on unpatterned AISI304 substrate. The profile height of the marked coating sections (red and teal rectangles on the left and right, respectively) is compared to that of the uncoated sec-

tion (accordingly colored rectangles in the middle) to determine the thickness of the lubricant coatings. The profiles related to the green lines are depicted directly below the respective micrograph. The height values on the y-axis are in μm

during friction testing against a 100Cr6 counter body over 1 h. According to Blau, the reference exhibits a type (c) run-in behavior, which is fittingly associated with unlubricated metals [25, 26]. Continuous asperity truncation leads to an increasingly conformal surface and causes an increase of the initial friction as well as the formation of wear particles, some of which are deposited in the surface grooves.

After extensive asperity removal, the counter body comes into contact with the low-lying, low-shear debris layer which could explain the drop after the first COF peak. Once most of the wear particles are removed from the contact, the second peak is possibly caused by abrasion from the remaining debris [26, 27]. Steady-state friction is reached after 300 cycles at a COF of 0.60. Concerning the coated samples,

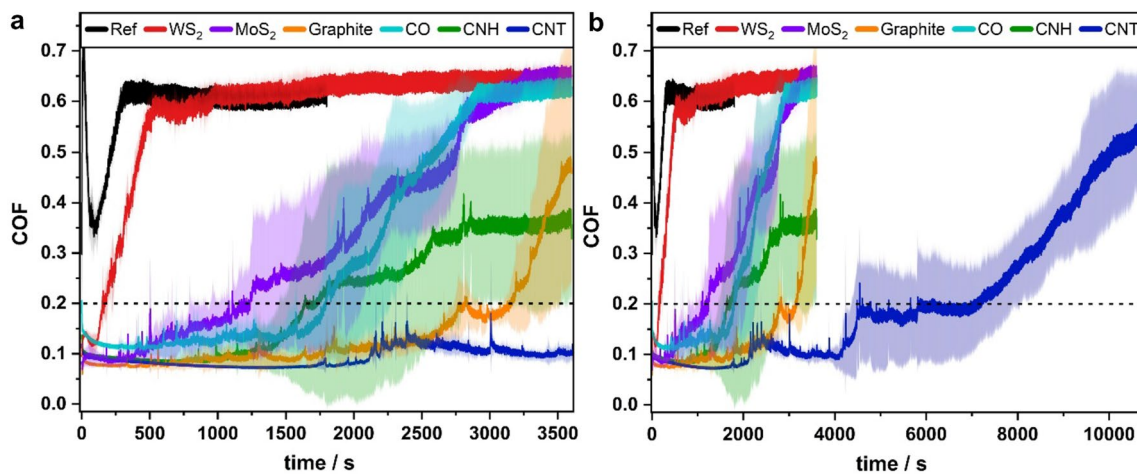


Fig. 3 **a** COF development of lubricant-coated and line-patterned substrates against a 100Cr6 ball at a load of 20 N over 3600 s (1 h) and **b** over 10,800 s (3 h). Friction testing was conducted at room

temperature and a relative humidity of 25–30%. The shaded areas correspond to the standard deviation of the respective sample. The dashed line represents the upper limit of effective solid lubrication

initially all show a significant improvement compared to the reference sample with COFs between 0.05 and 0.15. However, over the course of the experiments, the lubricity of the laser-patterned and coated samples degrades, and the lifetime depends strongly on the coating material. The lubricity of the two TMDs fades first. This is particularly true for WS_2 , whose COF increases immediately and sharply after only 100 s of sliding, reaching the reference COF after roughly 900 s. MoS_2 performs significantly better as it maintains a COF below 0.10 for roughly 350 s from where the COF slowly increases to the reference level after 3200 s. The discrepancy in the TMDs' friction behavior could be explained by a difference in shear strength. The poor performance of the TMD coatings in ambient conditions was to be expected due to the formation of MoO_3 and WO_3 , respectively.

Graphite shows highly effective lubricity, which declines slowly but steadily. After 3000 s, its COF surges sharply and a final value of 0.48 is reached after 3600 s. As defined by Aouadi et al., a COF below 0.2 is considered effective solid lubrication (marked by dashed line) since irreversible deformation of the contact surfaces is likely to occur for COF values above 0.2 [28]. On that basis, the CO and CNH coatings provide effective solid lubrication for roughly 1750s and graphite for about 3150 s. The fact that graphite lubricates at high load and a relative humidity of 25–30% is consistent with recent findings by Morstein et al. [6]. The best performing carbon nanoparticle coating is the CNT coating. From the beginning, the CNT coating maintains a lubricating steady-state with COF values between 0.07 and 0.10. After 2000s, the COF rises moderately to 0.16 including multiple localized peaks. After that, the COF decreases again and reaches a final value of just below 0.1 after 3600 s,

which corresponds to a friction reduction by a factor of 6 compared to the reference. The described peaks also appear in the curves of most other coatings, exclusively during the lubricating phase, and suggest adhesion, probably even material transfer according to Blau [26]. This phenomenon could also relate to temporary lubricant starvation in the contact that is followed by a replenishment of the contact with fresh lubricious particles from lower regions of the patterns (i.e., the particle reservoirs). A combination of both is also conceivable. To investigate how long the CNTs can maintain their lubricity under extreme load, the test duration was extended to 10,800 s (3 h) (Fig. 3b). After 4100 s, the CNTs' COF start to increase to just under 0.20 and somewhat stabilizes between 0.15 and 0.20. About another 3000 s later, the COF rises again, this time continuously and evenly until the end of the test. With 0.54, the final COF is still below the reference value of 0.60. CNT coatings provide effective solid lubrication against 100Cr6 at a load of 20 N over a period of 7100 s (almost 2 h), representing a lubrication extension by a factor of 2.3 compared to the graphite coating.

As shown by EDS mapping in Fig. 4 (bright green represents oxidation), applying a load of 20 N in the chosen experimental setup leads to severe oxidation of the reference wear track, which measures roughly 600 μm in width. The wear tracks of WS_2 and MoS_2 are even wider (750 μm and 650 μm , respectively) and exhibit oxidation of comparable magnitude. Compared to that, oxidation inside the wear tracks of CO, CNH is similarly severe, but they are narrower (both roughly 540 μm wide), while the graphite track is with 660 μm again wider. Considering the final COF values of graphite and CNH are lower than that of CO, this not reflected in the scale and oxidation state of the wear

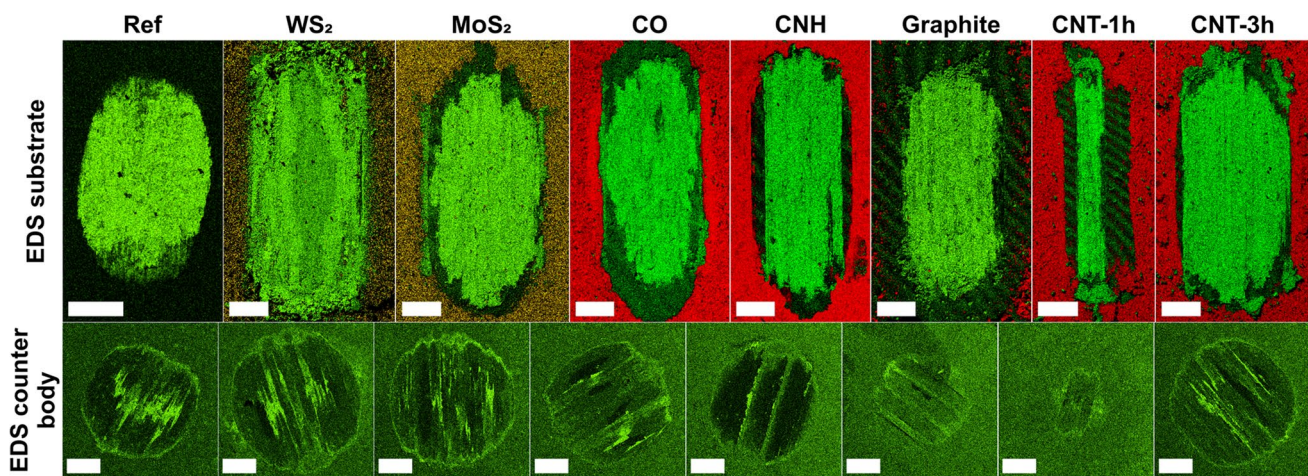


Fig. 4 EDS maps of the substrate wear tracks of the reference and the surfaces coated with WS_2 , MoS_2 , CO, CNH, graphite, CNT-1 h after friction testing against a 100Cr6 counter body for 3600 s at 20 N. Additionally, the EDS map of CNT-3 h after 10,800 s of testing is shown. Below, EDS maps of the wear tracks on the 100Cr6 counter

body surface after rubbing against the reference and the surfaces coated with WS_2 , MoS_2 , CO, CNH, graphite, CNT-1 h, CNT-3 h are depicted. In the EDS maps, green stands for oxygen, yellow for sulfur, and red for carbon. The scale bars are 250 μm in the EDS maps of the substrate wear tracks and otherwise 200 μm

tracks since they are comparable. Severe oxidation also occurs on the CNT-1 h wear track, however, at 150 μm , the oxidized strip is a quarter of the width of the reference. Due to effective lubrication, wear is milder and consequently, the enlargement of the real contact area is delayed, resulting in narrower oxidation regions. The low COF values of the CNTs after 1 h are remarkable considering the degree of substrate oxidation and the fact that no significant amounts of carbon are detected in the wear track. MacLucas et al. made similar findings after ball-on-disc friction testing on directionally ground and CNT-coated iron surfaces [29]. This further demonstrates, how little carbon is required to maintain an effective solid lubrication. After 3 h, the CNT-coated wear track is also heavily oxidized although its final COF is slightly below that of the other failed lubricant coatings. The wave-like patterns surrounding the wear tracks of graphite and CNT-1 h are generated by the Moiré effect, which is caused by a superimposition of the periodic surface pattern and the scanning electrons. In both cases, the occurrence of the Moiré effect indicates that the line patterns next to the oxidized stripes are at least partially intact.

Oxygen mapping is also used for the wear tracks on the counter bodies, primarily to assess the extent of their oxidation and their dimensions. Severely oxidized areas can be observed in the wear tracks of the reference, WS_2 , MoS_2 , CO, and CNT-3 h with center widths ranging from 600 (Ref) to 675 μm (MoS_2). Although the size of the CNH track is similar to the previously mentioned samples, there is only minor oxidation which is restricted to two thin stripes in the middle of the wear track. At roughly 450 μm , the graphite track is notably smaller and less oxidized. After friction testing using a similar tribological setup, Morstein

et al. observed the transfer of graphite-derived carbon from a graphite-coated iron substrate to a 100Cr6 counter body, which would explain the reduced wear and oxidation of our counter bodies [30]. Measuring 330 μm in width, the CNT-1 h track is roughly half as wide as the reference wear track and, thus, the smallest out of all counter body wear tracks. At the same time, the CNT-1 h wear track shows the least amount of oxidation (minor, if any), which agrees well with the superior tribological performance of the CNTs. This substantial improvement is probably due to remnants of CNT-derived carbon, transferred from the substrate surface to the counter body, therefore, forming a tribo-system that incorporates the acting shear stresses and protects the surface. However, this material transfer to the 100Cr6 counter body cannot be detected by EDS as the counter body contains about 1 wt.% of carbon and, therefore, it cannot be distinguished whether the detected carbon stems from transferred CNTs or from the counter body material. This becomes evident by comparing the carbon maps of the references' counter body track (Fig. 5a), which was never in contact with a carbon coating, and the corresponding CNT track (Fig. 5b) where carbon transfer is likely to have occurred.

3.2.2 Counter Body Material: Alumina

Figure 6a shows the COF development of the same solid lubricant coatings against an alumina counter body over 1 h. The run-in of the reference curve cannot be definitively assigned to a curve type, instead it shows characteristics of types (b) and (d). The curve most closely resembles type (d) with a COF drop after the second peak, as is characteristic for type (b). This agrees well with Blau,

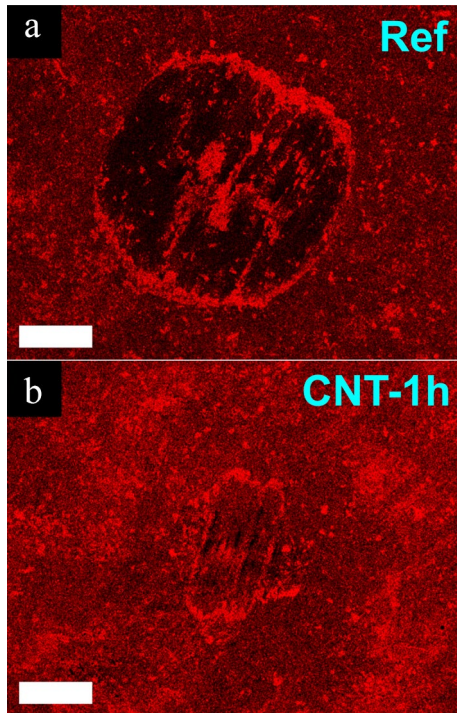


Fig. 5 EDS maps of the 100Cr6 counter body wear tracks after sliding against **a** the reference and **b** CNT-coated substrate for 3600 s at 20 N. In the EDS maps, red represents carbon. The scale bars are 200 μm

according to whom this behavior is often observed in ferrous or ferrous-nonferrous pairings, among others [26]. After running-in, the COF reaches a steady-state just

below 0.70 after 800 s [25]. Similar to testing against 100Cr6, the lubricity of the TMDs fails first and MoS_2 significantly outperforms WS_2 .

The COF development of the CNH and CO coatings is similar. After an initial COF drop, both enter a lubricating steady-state. During this stage, the COF of the CNH coating (< 0.10) is lower, yet starts to rise after 300 s, while the CO coating maintains lubricity longer at a slightly higher COF, however, it starts to increase more steeply after about 2500 s. After 3600 s, their COF values are around 0.60 and continue rising, but are still well below the reference value. Starting below 0.10, the COF of graphite starts to increase early, stabilizes after 2750 s and remains constant at 0.40 until the end of the test. It should be noted that, in contrast to sliding against 100Cr6, CO and CNH exhibit better lubricity than graphite for a majority of the first roughly 3000 s. The CNTs maintain a lubricating steady-state for more than 2000s, after which the COF starts to rise, reaching a final value of 0.24. After sliding against alumina for 3600 s, CNTs and graphite exhibit the lowest COF values of all coating materials. However, the CNT coating provides effective solid lubrication for over 3000 s compared to the 800 s of graphite which corresponds to lubrication extension by a factor of 3.8. At the same time, their lubricities are the least reproducible as expressed by substantial standard deviations and since they overlap, friction testing was prolonged to 10,800 s (3 h) (Fig. 6b). During the extension, the COF of both coatings increases gradually, however, that of graphite rises more steeply and matches the reference value after 6000 s, whereas the final COF of the CNT coating remains slightly below.

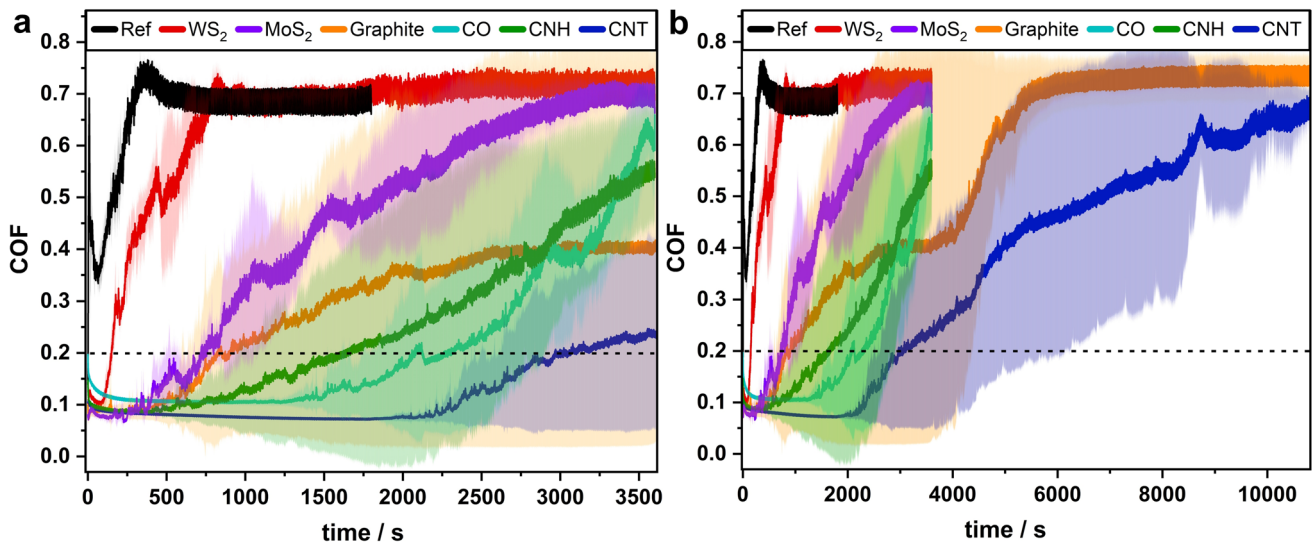


Fig. 6 a COF development of lubricant-coated and line-patterned substrates against an alumina ball at a load of 20 N over 3600 s (1 h) and **b** over 10,800 s (3 h). Friction testing was conducted at room

temperature and a relative humidity of 25–30%. The shaded areas correspond to the standard deviation of the respective sample. The dashed line represents the upper limit of effective solid lubrication

Regarding the alumina curves, the localized peaks occur significantly less frequently and are less pronounced compared to the 100Cr6 curves. This is in good agreement with Blau's adhesion hypothesis as 100Cr6 steel is considerably more reactive than alumina and thus both substrate and coating materials adhere more readily.

It is also worth noting that all carbon nanoparticle coatings, irrespective of counter body material, exhibit a type (f) run-in behavior. As shown in our previous work [29], CNT coatings are compacted during the initial phase of tribological loading, so that the COF decreases continuously during the early stage of running-in. This is followed by a lubricating steady-state which explains the development of a type (f) curve. Similar curve development suggests that particle compaction also occurs in CO and CNH coatings.

Figure 7 shows an overview of EDS maps, characterizing the resulting wear tracks on the substrates and the alumina counter bodies after friction testing. The extent of substrate oxidation and the oxidation width of the reference, WS₂, and MoS₂ tracks are almost identical to those wear tracks that were rubbed against 100Cr6. The CO- and CNH-coated wear tracks are also severely oxidized but narrower than those of the Ref and the TMD-coated surfaces at 365 μm and 330 μm for CO and CNH, respectively. That fact that the two wear tracks are similar in width aligns well with their COF development. They are also narrower than their corresponding wear tracks against 100Cr6. Although their COFs are below the Ref, no significant amounts of carbon are detected in the wear track center, merely traces on the edges of the oxidized

areas. Regarding the CNT- and graphite-coated wear tracks (after 1 h), the Moiré effect occurs again, this time, however, inside the tracks and slightly distorted, particularly in the case of graphite. This is a strong indication that the laser patterns have been largely preserved, which is confirmed by the respective CLS micrographs which are shown in Fig. S1 of the Supplementary Information. For both coatings, these images show lines of the original pattern remaining in much of the wear track, and they are usually at least partially filled with particles. Fittingly, EDS characterization also corroborates the presence of carbon in both wear tracks as well as on the edges, and no oxidation. These findings are in good agreement with those of MacLucas et al. who reported on the formation of CNT patches after conducting friction tests using a similar tribological setup with CNT-coated and line-patterned stainless-steel surfaces [11]. Subsequent EDS characterization also revealed no substrate oxidation, implying a complete separation of the sliding surfaces. The wire-like morphology of the CNTs fosters particle entanglement resulting in strong coherence of large particle sections. Furthermore, strong compression exerted by the counter body during sliding appears to bond the superficial patches with the particles in the reservoirs. As a result, the patches become mechanically anchored within the topographical minima of the surface pattern, leading to longer particle retention. Although graphite-derived carbon also remains in the wear track after 1 h, and CNT patch formation was observed at significantly lower loads, this phenomenon could be a contributing factor for the CNTs' superior high

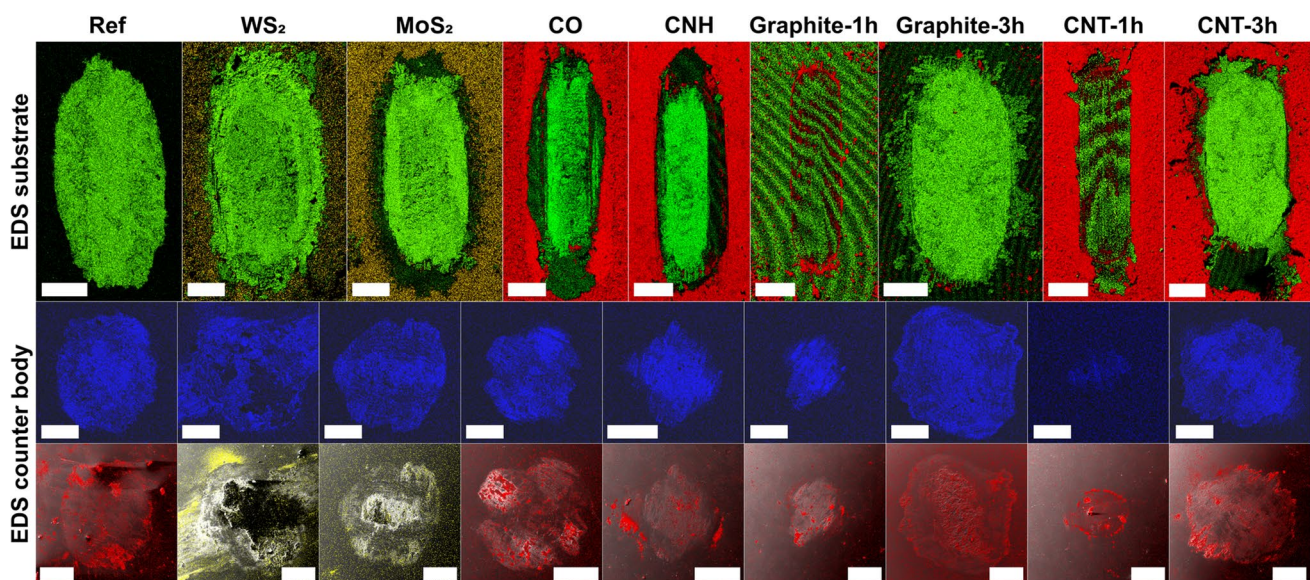


Fig. 7 EDS maps of the substrate wear tracks of the reference and the surfaces coated with WS₂, MoS₂, CO, CNH, graphite-1 h, graphite-3 h, CNT-1 h, CNT-3 h after friction testing against an alumina counter body for 3600 s or 10,800 s at 20 N. EDS maps and SEM/EDS overlays of the wear tracks on the alumina counter body surface

after rubbing against the reference and the surfaces coated with WS₂, MoS₂, CO, CNH, graphite-1 h, graphite-3 h, CNT-1 h, and CNT-3 h. In the EDS maps, blue stands for iron, yellow for sulfur, and red for carbon. The scale bar is 250 μm in the EDS maps of the substrate wear tracks and otherwise 200 μm

load lubricity compared to the other nanocarbons during high load friction. In contrast, COs aggregate strongly and form large clusters owing to their size and curvature, which are easily removed from the reservoirs and thus from the contact during sliding, leading to relatively fast lubricant depletion [3]. After 3 h, the CNT lubrication is about to fade completely, whereas the graphite lubrication has already failed after 2 h. Despite comparable degrees of oxidation, the wear tracks of graphite and CNT are also slightly narrower (570 μm and 540 μm , respectively) than that of the reference which is expected due to the initial lubrication.

As can be derived from the standard deviation of the COF development of graphite-1 h and CNT-1 h, the wear tracks differ to a degree, however, we consider the presented wear tracks to be the most representative (the CLS micrographs of all graphite-1 h wear tracks are provided in the Supplementary Information, Fig. S2).

EDS maps of iron (blue), sulfur (yellow), and carbon (red) are used to assess material transfer from the substrate surface to the alumina counter body. With respect to iron, the material transfer from the AISI304 substrate to the counter body material is considerable in the case of Ref, WS₂, MoS₂, CO, graphite-3 h, and CNT-3 h. In the case of CNH, the iron transfer is still substantial, but less pronounced compared to the previously mentioned samples. Even less iron is transferred to the counter body for graphite-1 h and hardly any iron transfer to the counter body is observable for CNT-1 h. In addition to that, sulfur mapping was carried out in the case of the TMDs, and notable amounts are found at the edges of the counter body wear tracks after rubbing against the WS₂ coating, whereas none is detected for MoS₂.

Carbon is measured in varying quantities on the alumina surface due to different degrees of atmospheric contamination. This is made particularly evident by the carbon map of the Ref sample which indicates the presence of carbon although it was never in contact with a carbon-coated surface. This is corroborated by the shading caused by large dirt particles which are non-compressed unlike the transferred carbon. Therefore, solely increased carbon concentrations (bright red) either within the wear tracks or at the edges compared to the surrounding area were considered as transferred material. Concerning graphite-3 h, the carbon quantity inside of its wear tracks is not increased compared to the surrounding areas except for minute remnants at the edges. On the CNT-3 h counter body, carbon concentrations at the edges are clearly elevated, suggesting carbon transfer, albeit minor.

It would explain why the final COF of CNT-3 h is marginally lower compared to that of graphite-3 h. The carbon concentrations are minimally elevated inside the counter body tracks of CO and CNH. In addition, the CNH track also shows considerable amounts of transferred carbon just outside of the wear track edges. The carbon traces are likely

responsible for their slightly lower COF compared to the reference. Overall, the carbon transfer, especially inside the wear tracks, is comparable and this is reflected by a similar COF development. After rubbing against the graphite coating for 1 h, EDS mapping clearly shows small carbon patches inside the wear track that outlasted the frictional stress and continue to lubricate. The largest amount of carbon, however, is found on the counter body wear track of CNT-1 h, both inside and at the edges, along with a large dirt particle in the middle of the track. During previous works involving CNT coatings sliding against alumina in similar conditions, we observed that material transfer from substrate to alumina was either minor or non-existent [11, 29]. According to the mechanism formulated by MacLucas and co-workers, the dangling bonds are quickly saturated by atmospheric compounds [29]. It is conceivable, however, that CNT degradation is greatly enhanced under high loads (20 N) and therefore, more reactive dangling bonds are formed. This could explain an increased transfer of CNT-derived carbon in contrast to earlier studies conducted at lower loads (100 mN). Overall, a strong correlation between COF development and material transfer from the substrate to the alumina counter body can be observed: The higher the carbon transfer, particularly inside the wear track, the lower the COF and the iron transfer.

4 Conclusion

In this study, comparative friction testing of three types of carbon nanoparticle coatings and conventional solid lubricant coatings is conducted on line-patterned AISI 304 substrates against two technically relevant counter body materials (100Cr6 and alumina) at a load of 20 N. Regardless of counter body material, the results show the lubricity of the CNT coating to be superior compared the other solid lubricants in terms of COF and lubrication duration.

Against 100Cr6, the CNT-coated substrate exhibits severe oxidation, whereas on the counter body surface, oxidation is minor. Given the severity of the substrate oxidation, it is remarkable that the COF is still around 0.1, demonstrating how little carbon is required in the contact to provide effective solid lubrication. In addition, long-term testing reveals that the CNTs' COF is still below that of the reference. The numerous localized peaks in the COF curves as well the low extent of counter body wear track oxidation are strong indicators of carbon transfer. Furthermore, CNH and graphite are also able to maintain lubrication against 100Cr6, however, their COF values are higher and substrate oxidation is significantly enhanced.

After sliding against alumina for 3600 s, no oxidation is detected on the CNT-coated substrate, which is in accordance with a previous study by MacLucas et al. where the

formation of surface-separating CNT patches was observed. This phenomenon might contribute to the outperformance of CNT coatings against the other solid lubricant coatings. This also corresponds to the fact that, if at all, only small amounts of iron are transferred along with significant amounts of carbon. At the same time, graphite also sustains lubricity but at a higher COF level. In both cases, the original line-patterns are at least partially retained. During long-term testing against alumina, the COF of graphite rises steeply and quickly reaches the reference value, whereas in the case of CNT, the COF increases more slowly and gradually, and the final COF remains below the reference level.

The results of this work demonstrate the potential of CNT-based solid lubrication systems for high load applications. Our findings further illustrate the efficacy of the reservoir effect achieved by combining lubricant coatings with well-defined surface patterns for extending the lubricity of conventional solid lubricant coatings in various industrial applications.

Supplementary Information The online version contains supplementary material available at <https://doi.org/10.1007/s11249-024-01837-5>.

Author Contributions Conceptualization: T.M., S.S., C.G.; Formal analysis: T.M.; Investigation: T.M., P.L., S.S.; Writing—original draft: T.M., P.G.G.; Project administration: T.M., P.G.G., S.S.; Funding acquisition, supervision: C.G., F.M.; Writing—review and editing: S.S., P.G.G., C.G. and F.M. All authors reviewed and approved the final version of the manuscript.

Funding Open Access funding enabled and organized by Projekt DEAL. This work was financially supported by the German Research Foundation (Deutsche Forschungsgemeinschaft, DFG) within the projects MU 959/47-1 and the State of Saarland from the European Regional Development Fund (Europäischen Fonds für Regionale Entwicklung, EFRE) within the ZuMat project. Funding for the PFIB/SEM instrument by DFG is greatly acknowledged (INST 256/510-1 FUGG).

Data Availability The research data supporting the findings presented in this paper will be made available by the corresponding authors upon reasonable request.

Declarations

Conflict of interest The authors declare that they have no conflicts of interest.

Open Access This article is licensed under a Creative Commons Attribution 4.0 International License, which permits use, sharing, adaptation, distribution and reproduction in any medium or format, as long as you give appropriate credit to the original author(s) and the source, provide a link to the Creative Commons licence, and indicate if changes were made. The images or other third party material in this article are included in the article's Creative Commons licence, unless indicated otherwise in a credit line to the material. If material is not included in the article's Creative Commons licence and your intended use is not permitted by statutory regulation or exceeds the permitted use, you will need to obtain permission directly from the copyright holder. To view a copy of this licence, visit <http://creativecommons.org/licenses/by/4.0/>.

References

- Holmberg, K., Erdemir, A.: Influence of tribology on global energy consumption, costs and emissions. *Friction* **5**, 263–284 (2017). <https://doi.org/10.1007/s40544-017-0183-5>
- Rosenkranz, A., Costa, H.L., Baykara, M.Z., Martini, A.: Synergetic effects of surface texturing and solid lubricants to tailor friction and wear – a review. *Tribol. Int.* **155**, 106792 (2021). <https://doi.org/10.1016/j.triboint.2020.106792>
- MacLucas, T., Daut, L., Grützmacher, P., Guitar, M.A., Presser, V., Gachot, C., Suarez, S., Mücklich, F.: Influence of structural depth of laser-patterned steel surfaces on the solid lubricity of carbon nanoparticle coatings. *Friction* **11**, 1276–1291 (2023). <https://doi.org/10.1007/s40544-022-0664-z>
- Burriss, D.L., Sawyer, W.G.: A low friction and ultra low wear rate PEEK/PTFE composite. *Wear* **261**, 410–418 (2006). <https://doi.org/10.1016/j.wear.2005.12.016>
- Scharf, T.W., Prasad, S.V.: Solid lubricants: a review. *J. Mater. Sci.* **48**, 511–531 (2013). <https://doi.org/10.1007/s10853-012-7038-2>
- Morstein, C.E., Klemenz, A., Dienwiebel, M., Moseler, M.: Humidity-dependent lubrication of highly loaded contacts by graphite and a structural transition to turbostratic carbon. *Nat. Commun.* **13**, 5958 (2022). <https://doi.org/10.1038/s41467-022-33481-9>
- Vazirisereshk, M.R., Martini, A., Strubbe, D.A., Baykara, M.Z.: Solid lubrication with MoS₂: a review. *Lubricants* (2019). <https://doi.org/10.3390/LUBRICANTS7070057>
- Grützmacher, P.G., Schranz, M., Hsu, C.J., Bernardi, J., Steiger-Thirsfeld, A., Hensgen, L., Rodríguez Ripoll, M., Gachot, C.: Solid lubricity of WS₂ and Bi₂S₃ coatings deposited by plasma spraying and air spraying. *Surf. Coat. Technol.* (2022). <https://doi.org/10.1016/j.surfcoat.2022.128772>
- Grützmacher, P.G., Suarez, S., Tolosa, A., Gachot, C., Song, G., Wang, B., Presser, V., Mücklich, F., Anasori, B., Rosenkranz, A.: Superior wear-resistance of Ti₃C₂T_x multilayer coatings. *ACS Nano* **15**, 8216–8224 (2021). <https://doi.org/10.1021/acsnano.1c01555>
- Reinert, L., Varenberg, M., Mücklich, F., Suárez, S.: Dry friction and wear of self-lubricating carbon-nanotube-containing surfaces. *Wear* (2018). <https://doi.org/10.1016/j.wear.2018.03.021>
- MacLucas, T., Leonhard-Trautmann, P., Suarez, S., Mücklich, F.: Long-term lubricity of carbon nanoparticle coatings on periodically laser-patterned metallic surfaces. *Tribol. Lett.* **70**, 123 (2022). <https://doi.org/10.1007/s11249-022-01667-3>
- Reinert, L., Lasserre, F., Gachot, C., Grützmacher, P., MacLucas, T., Souza, N., Mücklich, F., Suarez, S.: Long-lasting solid lubrication by CNT-coated patterned surfaces. *Sci. Rep.* **7**, 42873 (2017). <https://doi.org/10.1038/srep42873>
- Choudhary, N., Hwang, S., Choi, W.: Carbon Nanomaterials: A Review. In: Bhushan, B., Luo, D., Schrickler, S.R., Sigmund, W., Zauscher, S. (eds.) *Handbook of Nanomaterials Properties*, pp. 709–769. Springer, Berlin, Heidelberg (2014)
- Rosenkranz, A., Grützmacher, P.G., Gachot, C., Costa, H.L.: Surface texturing in machine elements—a critical discussion for rolling and sliding contacts. *Adv. Eng. Mater.* **21**, 1900194 (2019). <https://doi.org/10.1002/adem.201900194>
- Rosenkranz, A., Grützmacher, P.G., Murzyn, K., Mathieu, C., Mücklich, F.: Multi-scale surface patterning to tune friction under mixed lubricated conditions. *Appl. Nanosci.* (2019). <https://doi.org/10.1007/s13204-019-01055-9>
- Schäfer, C., Reinert, L., MacLucas, T., Grützmacher, P., Merz, R., Mücklich, F., Suarez, S.: Influence of surface design on the solid lubricity of carbon nanotubes-coated steel surfaces. *Tribol. Lett.* **66**, 1–15 (2018)

17. Lasagni, A.F., Gachot, C., Trinh, K.E., Hans, M., Rosenkranz, A., Roch, T., Eckhardt, S., Kunze, T., Bieda, M., Günther, D., Lang, V., Mücklich, F.: Direct laser interference patterning, 20 years of development: from the basics to industrial applications. In: Proc. SPIE 10092, Laser-based Micro- and Nanoprocessing XI. p. 1009211 (2017). <https://doi.org/10.1117/12.2252595>
18. Braun, P., Grützmacher, P., Frohnäpfel, L., Mücklich, F., Durst, K.: Nanoscale patterning of metallic surfaces with laser patterned tools using a nanoimprinting approach. *Appl. Surf. Sci.* (2023). <https://doi.org/10.1016/j.apsusc.2022.155786>
19. Müller, D.W., Fox, T., Grützmacher, P.G., Suarez, S., Mücklich, F.: Applying ultrashort pulsed direct laser interference patterning for functional surfaces. *Sci. Rep.* **10**, 3647 (2020). <https://doi.org/10.1038/s41598-020-60592-4>
20. MacLucas, T., Schütz, S., Suarez, S., Mücklich, F.: Surface protection of austenitic steels by carbon nanotube coatings. *Surf. Topogr.* **6**, 14005 (2018)
21. Voevodin, A.A., Bultman, J., Zabinski, J.S.: Investigation into three-dimensional laser processing of tribological coatings. *Surf. Coat. Technol.* **107**, 12–19 (1998). [https://doi.org/10.1016/S0257-8972\(98\)00543-X](https://doi.org/10.1016/S0257-8972(98)00543-X)
22. Voevodin, A.A., Zabinski, J.S.: Laser surface texturing for adaptive solid lubrication. *Wear* **261**, 1285–1292 (2006). <https://doi.org/10.1016/j.wear.2006.03.013>
23. Rosenkranz, A., Grützmacher, P.G., Espinoza, R., Fuenzalida, V.M., Blanco, E., Escalona, N., Gracia, F.J., Villarroel, R., Guo, L., Kang, R., Mücklich, F., Suarez, S., Zhang, Z.: Multi-layer Ti₃C₂T_x-nanoparticles (MXenes) as solid lubricants—role of surface terminations and intercalated water. *Appl. Surf. Sci.* **494**, 13–21 (2019). <https://doi.org/10.1016/j.apsusc.2019.07.171>
24. Zeiger, M., Jäckel, N., Aslan, M., Weingarh, D., Presser, V.: Understanding structure and porosity of nanodiamond-derived carbon onions. *Carbon NY* **84**, 584–598 (2015). <https://doi.org/10.1016/j.carbon.2014.12.050>
25. Blau, P.J.: On the nature of running-in. *Tribol. Int.* **38**, 1007–1012 (2005). <https://doi.org/10.1016/j.triboint.2005.07.020>
26. Blau, P.J.: *Friction Science and Technology*. CRC Press, Boca Raton (2008)
27. Blau, P.J.: Interpretations of the friction and wear break-in behavior of metals in sliding contact. *Wear* **71**, 29–43 (1981)
28. Aouadi, S.M., Gao, H., Martini, A., Scharf, T.W., Muratore, C.: Lubricious oxide coatings for extreme temperature applications: a review. *Surf. Coat. Technol.* **257**, 266–277 (2014)
29. MacLucas, T., Klemenz, A., Grünewald, P., Presser, V., Mayrhofer, L., Moras, G., Suarez, S., Dienwiebel, M., Mücklich, F., Moseler, M.: Multiwall carbon nanotubes for solid lubrication of highly loaded contacts. *ACS Appl. Nano Mater.* **6**, 1755–1769 (2023). <https://doi.org/10.1021/acsanm.2c04729>
30. Morstein, C.E., Dienwiebel, M.: Graphite lubrication mechanisms under high mechanical load. *Wear* **477**, 203794 (2021). <https://doi.org/10.1016/j.wear.2021.203794>

Publisher's Note Springer Nature remains neutral with regard to jurisdictional claims in published maps and institutional affiliations.